LETTER

doi:10.1038/nature11223

Synthetic homeostatic materials with chemo-mechano-chemical self-regulation

Ximin He[1,2], Michael Aizenberg[2], Olga Kuksenok[3], Lauren D. Zarzar[4], Ankita Shastri[4], Anna C. Balazs[3] & Joanna Aizenberg[1,2,4]

Living organisms have unique homeostatic abilities, maintaining tight control of their local environment through interconversions of chemical and mechanical energy and self-regulating feedback loops organized hierarchically across many length scales[1–7]. In contrast, most synthetic materials are incapable of continuous self-monitoring and self-regulating behaviour owing to their limited single-directional chemomechanical[7–12] or mechanochemical[13,14] modes. Applying the concept of homeostasis to the design of autonomous materials[15] would have substantial impacts in areas ranging from medical implants that help stabilize bodily functions to 'smart' materials that regulate energy usage[2,16,17]. Here we present a versatile strategy for creating self-regulating, self-powered, homeostatic materials capable of precisely tailored chemo-mechano-chemical feedback loops on the nano- or microscale. We design a bilayer system with hydrogel-supported, catalyst-bearing microstructures, which are separated from a reactant-containing 'nutrient' layer. Reconfiguration of the gel in response to a stimulus induces the reversible actuation of the microstructures into and out of the nutrient layer, and serves as a highly precise 'on/off' switch for chemical reactions. We apply this design to trigger organic, inorganic and biochemical reactions that undergo reversible, repeatable cycles synchronized with the motion of the microstructures and the driving external chemical stimulus. By exploiting a continuous feedback loop between various exothermic catalytic reactions in the nutrient layer and the mechanical action of the temperature-responsive gel, we then create exemplary autonomous, self-sustained homeostatic systems that maintain a user-defined parameter—temperature—in a narrow range. The experimental results are validated using computational modelling that qualitatively captures the essential features of the self-regulating behaviour and provides additional criteria for the optimization of the homeostatic function, subsequently confirmed experimentally. This design is highly customizable owing to the broad choice of chemistries, tunable mechanics and its physical simplicity, and may lead to a variety of applications in autonomous systems with chemo-mechano-chemical transduction at their core.

The survival of organisms relies on homeostatic functions such as the maintenance of stable body temperature, blood pressure, pH and sugar levels[1,3,5–7]. This remarkable self-regulatory capability can be traced to macromolecular components that convert chemical processes into nano- or microscale motion and vice versa, such as ATP synthesis[5] and muscle contraction[4,7], thereby mechanically mediating the coupling of a wide range of disparate chemical signals[1,2]. Despite its importance in living systems, the concept of homeostasis and self-regulation has not been applied extensively to man-made materials, with the result that many are energy inefficient or fail when subject to minor perturbations. Synthetic materials typically sense or actuate only along a single chemomechanical[8–12] ($C \rightarrow M$) or mechanochemical[13,14] ($M \rightarrow C$) route, and are generally incapable of integration into feedback mechanisms that necessarily incorporate both pathways ($C_1 \rightarrow M \rightarrow C_2$ or $C \rightleftarrows M$). There are a few stimuli-responsive drug delivery systems, which utilize chemo-mechano-chemical elements that lead to the release of certain molecules to target locations[18–20]. Select oscillating and non-oscillating reactions have been coupled to reversible mechanical responses[21–25], yet systems that are driven by such a limited chemical repertoire lack versatility and tunability. Despite substantial efforts, artificial chemomechanical systems capable of integration within hierarchical regimes, taking advantage of compartmentalization and partition[26], and offering smooth coupling of microscopic and macroscopic signals with fast mechanical action[4] and a wide range of chemical inputs and outputs remain a highly desired but elusive goal[16,17]. In response to these challenges, we describe here a new materials platform that can be designed to mediate a variety of homeostatic feedback loops. The system, which we call SMARTS (self-regulated mechanochemical adaptively reconfigurable tunable system), reversibly transduces external or internal chemical inputs into user-defined chemical outputs via the on/off mechanical actuation of microstructures.

The general, customizable design of SMARTS is presented in Fig. 1a. Partly embedded in a hydrogel 'muscle', high-aspect-ratio 'skeletal'

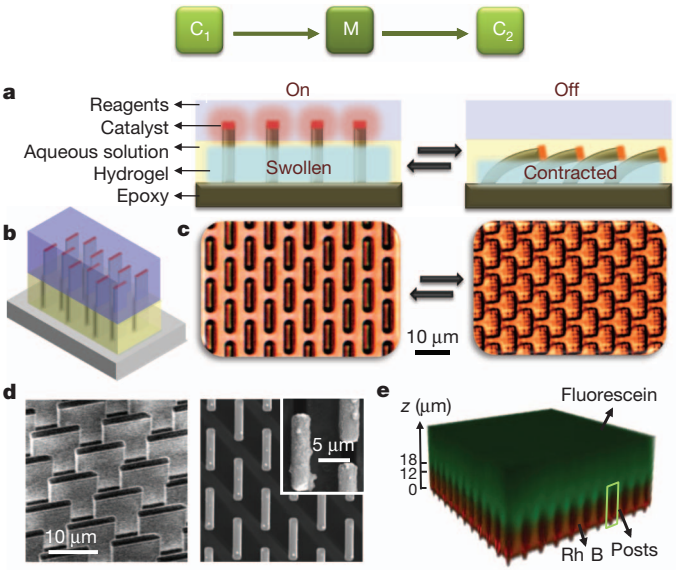

Figure 1 | General design of SMARTS. **a**, Cross-section schematic. **b**, Three-dimensional schematic. **c**, Top-view microscope images of upright and bent microfins corresponding to on (left) and off (right) reaction states. **d**, Forty-five-degree side-view (left) and top-view (right) scanning electron microscope images of 2-μm-wide, 10-μm-long, 18-μm-high microfins with the catalyst particles on tips (inset). **e**, Three-dimensional confocal microscope image of a hydrogel-embedded, 18-μm-tall post array immersed in a bilayer liquid labelled with fluorescein and rhodamine B, showing the interface height to be 12 μm (Supplementary Fig. 2).

[1]School of Engineering and Applied Sciences, Harvard University, Cambridge, Massachusetts 02138, USA. [2]Wyss Institute for Biologically Inspired Engineering, Harvard University, Cambridge, Massachusetts 02138, USA. [3]Department of Chemical and Petroleum Engineering, University of Pittsburgh, Pittsburgh, Pennsylvania 15260, USA. [4]Department of Chemistry and Chemical Biology, Harvard University, Cambridge, Massachusetts 02138, USA.

microstructures with a catalyst or reagent affixed to the tips reversibly actuate as the gel swells or contracts in response to a chemical stimulus (C_1). When this system is immersed in a liquid bilayer, this mechanical action (M) moves the catalyst into and out of a top layer of reactants (the nutrient layer), such that a chemical reaction (C_2) is turned on when the microstructures straighten and turned off when they bend, realizing a synchronized cascade of chemomechanical energy interconversions ($C_1 \rightarrow M \rightarrow C_2$). We built such a system using an epoxy microfin array (Fig. 1b) that reconfigures between upright and bent states (Fig. 1c) when the volume of the hydrogel changes. The catalyst or reagent of choice was physically adsorbed or chemically attached to the tips of the microstructures (Fig. 1d and Supplementary Fig. 1). The formation of a stable bilayer configuration was achieved in either a biphasic system or in a microfluidic device (Supplementary Fig. 2), and the position of the interface was determined by confocal microscopy using fluorescently labelled liquids (Fig. 1e).

Using this design, we first characterized and optimized a number of externally regulated $C_1 \rightarrow M \rightarrow C_2$ systems which show that SMARTS can be tailored to a broad range of coupled chemomechanical and mechanochemical events (Fig. 2). We incorporated microstructures actuated by a pH-responsive hydrogel, poly(acrylamide-*co*-acrylic acid)[27], into a microfluidic channel[28] and used laminar flow to generate a stable liquid bilayer on top of the microstructured surface (Supplementary Fig. 2). Using periodic changes in pH in the bottom layer as the stimulus (S), we realized chemo-mechano-chemical cycles of the type $(S_{on} \rightarrow C_1 \rightarrow M_{up} \rightarrow C_2) \rightarrow (S_{off} \rightarrow C_{-1} \rightarrow M_{bent} \nrightarrow C_2) \rightarrow (S_{on} \rightarrow \cdots)$, where S_{on} and S_{off} correspond to pH change, C_1 and C_{-1} respectively denote deprotonation of the acrylic acid and protonation of the acrylate moieties, M_{up} and M_{bent} denote the movement of the microstructures between the two liquid layers, and C_2 denotes various reactions triggered in the top layer (Fig. 2).

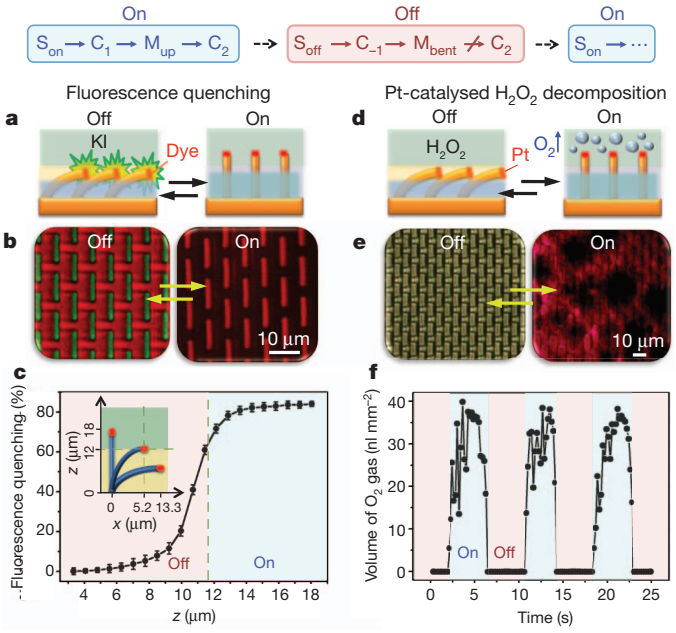

Figure 2 | Oscillations in exemplary chemical reactions triggered by pH changes. a–c, Fluorescence quenching. **a**, Schematic. **b**, Confocal microscope images showing green fluorescence of fluorescein on the tips of bent fins that disappears as fins enter the quenching potassium iodide (KI) layer. The red colour results from the presence of rhodamine B in the bottom layer. **c**, Fluorescence intensity as a function of the tip position (z). No fluorescence quenching occurs in the controls containing no potassium iodide in the top layer (Supplementary Fig. 3). Error bars, s.d.; $n = 4$. **d–f**, Pulsed, platinum-catalysed decomposition of hydrogen peroxide (H_2O_2). **d**, Schematic. **e**, Optical microscope images showing intermittent oxygen-bubble generation when the catalyst-bearing tips enter the layer of hydrogen peroxide. The colours arise from the pH indicator bromophenol blue. No bubbles form in the controls, which lack platinum catalysts (Supplementary Fig. 4). **f**, Time-resolved gas generation synchronous with the actuation of the fins.

To determine optimal conditions allowing the microstructures to pass sufficiently far across the fluidic interface (Fig. 2a, b), we applied fluorescein to the microstructure tips and observed the on/off states of fluorescein quenching by potassium iodide in the nutrient layer. By tracking the progress of both the chemical reaction and the motion of the microstructures (Fig. 2c and Supplementary Fig. 3), we demonstrated that the quenching started at almost the exact moment the 18-μm-tall tips crossed the ~12-μm-high interface into the layer of reagents, and ceased as the tips crossed again upon leaving the potassium iodide solution. The high level of chemomechanical coordination of SMARTS therefore provides both a precise and controllable way to use mechanical action to alter and affect dynamics of chemical systems and a basis for the design of much more complex, compartmentalized[2,16,17,26] chemo-mechano-chemical interactions.

Not only is this mechanical mediation inherently precise, but the system's response is also fast, allowing for rapid switching of an induced chemical reaction. We demonstrated, for example, that the pulsed generation of oxygen gas bubbles ($\sim 35\ nl\ mm^{-2}\ s^{-1}$) by a platinum-catalysed hydrogen peroxide decomposition reaction, $2H_2O_2 \xrightarrow{Pt} O_2 + 2H_2O$ (Fig. 2d–f, Supplementary Movie 1 and Supplementary Fig. 4), can be switched on and off entirely within a fraction of a second, in synchrony with the driving chemical stimulus. This system can also be designed to regulate much more complex, multicomponent enzymatic processes occurring in delicate, biologically relevant conditions. The variety of switchable C_2 reactions is complemented by the customizability of the hydrogel response, which can be tailored to a wide range of stimuli, such as pH, heat, light and glucose or other metabolic compounds, making it possible to mix and match chemical signals at will.

Of particular interest and potential importance is the ability to design self-regulated, autonomous $C_1 \rightarrow M \rightarrow C_2$ systems in which the chemical output signal is matched with the stimulus of the responsive hydrogel. Such a system would have homeostatic behaviour owing to the possibility of a complete, continuous feedback loop, $C \rightarrow M \rightarrow C \rightarrow M \rightarrow \cdots$ or $C \rightleftarrows M$ (Fig. 3a). We demonstrated this unique capacity by creating multiple self-powered, self-regulated oscillating systems in which the mechanical action of a temperature-responsive gel, poly(*N*-isopropylacrylamide), was coupled to several exemplary exothermic catalytic reactions:

(i) hydrosilylation of 1-hexene with triethylsilane catalysed by H_2PtCl_6 (Et, ethyl)

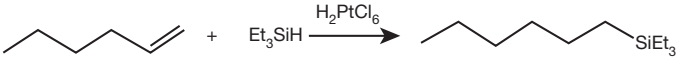

(ii) hydrosilylation of 1-hexene with diphenylsilane catalysed by H_2PtCl_6 (Ph, phenyl)

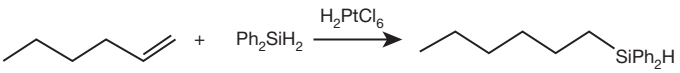

(iii) decomposition of cumene hydroperoxide catalysed by Ph_3CPF_6

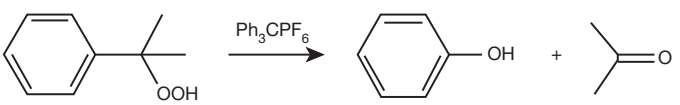

(iv) 'click' reaction between octylazide and phenylacetylene catalysed by $Cu(PPh_3)_2NO_3$

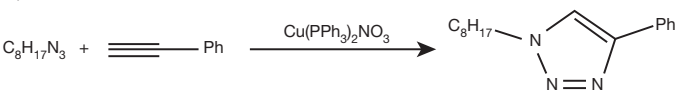

Below the lower critical solution temperature (LCST), the thermally responsive hydrogel swells, the embedded microstructures straighten

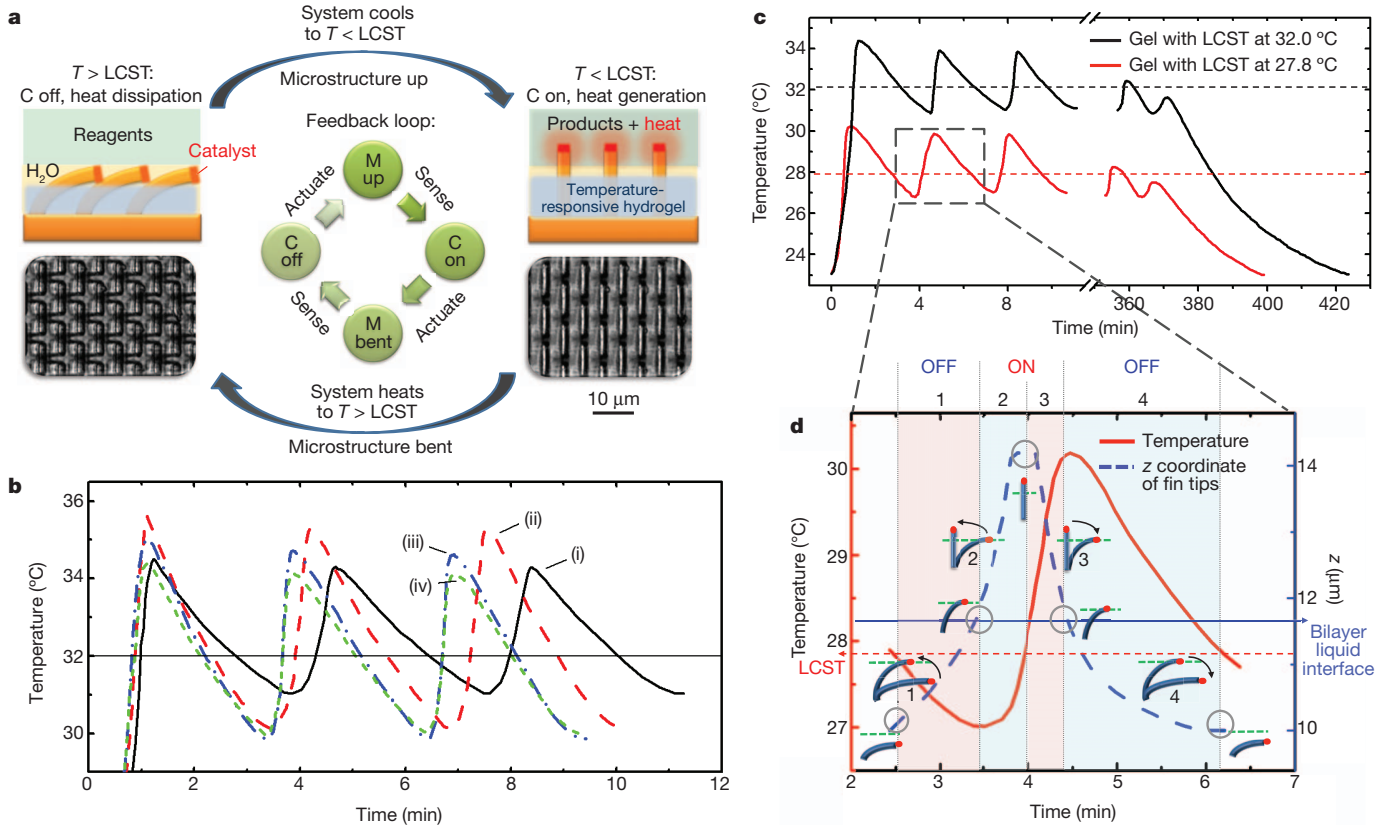

Figure 3 | Homeostasis in SMARTS via self-regulated chemo-thermo-mechanical feedback loops. **a**, Schematic of the temperature-regulating SMARTS showing a C ⇄ M feedback loop, in which mechanical action of temperature-responsive gel is coupled with an exothermic reaction. The side-view schematic and top-view microscope images depict on/off states of the reaction in the top layer. **b**, Temperature oscillations arising from different exothermic reactions driven by temperature-responsive poly(*N*-isopropylacrylamide) gel: (i), (ii), hydrosilylation of 1-hexene with triethylsilane (i) and diphenylsilane (ii); (iii) decomposition of cumene hydroperoxide; (iv) 'click' reaction between octylazide and phenylacetylene. **c**, Comparison between temperature oscillations using hydrogels with different LCSTs: 32.0 °C (black line) and 27.8 °C (red line). The control without catalyst did not maintain temperature and quickly cooled (Supplementary Fig. 8). **d**, Time-resolved temperature and vertical coordinate (z) of microfin tips for the system with LCST = 27.8 °C. Note the phase shift between the two curves. Inserts show schematic fin configurations.

and their catalyst-functionalized tips enter the reagent layer, triggering an exothermic reaction; when the temperature increases to $T > \mathrm{LCST}$ as a result of the generated heat, it triggers contraction of the hydrogel, removing the microstructures from the reagents; when the temperature falls to $T < \mathrm{LCST}$ again, the cycle restarts, giving rise to continuous, self-regulated C ⇄ M oscillations (Fig. 3a). All these systems behave as autonomous thermal regulators that, within a very narrow range, maintain a local temperature, which is determined by the LCST of the hydrogel (Fig. 3b). For example, when poly(*N*-isopropylacrylamide) hydrogel[29] (LCST = 32.0 °C) was used to switch reaction (i), the local temperature fluctuated between 31.0 and 33.8 °C (Fig. 3c and Supplementary Fig. 5). When we modified the poly(*N*-isopropylacrylamide) with 5% butyl methacrylate[30], to reduce the LCST to 27.8 °C, the local temperature range shifted to 27.1–29.7 °C (Fig. 3c, d). This robust self-contained feedback system, which is <70 μm thick, regulates the temperature of a 0.64-cm^2 surface for ~6 h (4.20 min per cycle for 95 cycles), with an initial input of only 4.0 μl of reactants as fuel (Supplementary Movie 2). With periodic replenishment of reactants, it can in principle continue to function almost indefinitely. The oscillation amplitude and period vary depending on the reactions' exothermicity and kinetics (see discussion below and Supplementary Figs 6–8).

To capture essential features of the self-regulating, oscillatory behaviour seen in the experiments and assess the contributions of different variables, we developed a hybrid computational approach to modelling microstructures that are embedded in a thermo-responsive gel and interact with an overlying layer of reagents (Supplementary Fig. 9 and Supplementary Information). This approach is based on the gel lattice spring model[31–33], which describes the elastodynamics of the gel layer (Fig. 4a). Simulations show that the phase trajectory of the vertical (z) coordinate of the microstructure tips, $z_{\mathrm{tip}}(T)$ (Fig. 4b), develops into a stable limit cycle, corresponding to robust, self-sustained oscillations (Fig. 4c). By focusing on a single oscillation cycle (Fig. 4d), we see that, in agreement with the experiments (Fig. 3c), the temperature of the system decreases when the tips are below the bilayer interface and increases when they are above this surface, resulting in a phase shift (of about one-third of the oscillation period) between the oscillations in temperature and tip position. Furthermore, at any temperature within the oscillation cycle, z_{tip} can attain one of two possible values, such that for the same temperature the tips are higher during heating and lower during cooling: $z_{\mathrm{tip}}^{\mathrm{heat}}(T^*) > z_{\mathrm{tip}}^{\mathrm{cool}}(T^*)$ (Fig. 4d; the same behaviour is observed in experiments, as seen in Fig. 3d). This feature is also evident in Fig. 4b, where the upper portion of the limit cycle corresponds to the tips being located above the interface (above the green line) and to the increase in temperature (marked by the red arrow pointing to the right), and the lower portion corresponds to the tips being located below the interface and to the decrease in temperature (marked by the red arrow pointing to the left). The bistability seen in Fig. 4d, as well as the negative feedback provided by the localized reaction, results in the oscillations seen in Figs 3 and 4. Notably, bistability has been shown to have a key role in various self-oscillating gels[21,22]; for example, bistability in the permeability of a gel membrane[21] or spatial bistability in pH-responsive gels[22] results in distinct chemomechanical oscillations.

Our model can be used to estimate trends in homeostatic behaviour based on tunable variables. For example, the modelling suggested (Supplementary Fig. 10) that the homeostatic temperature and the

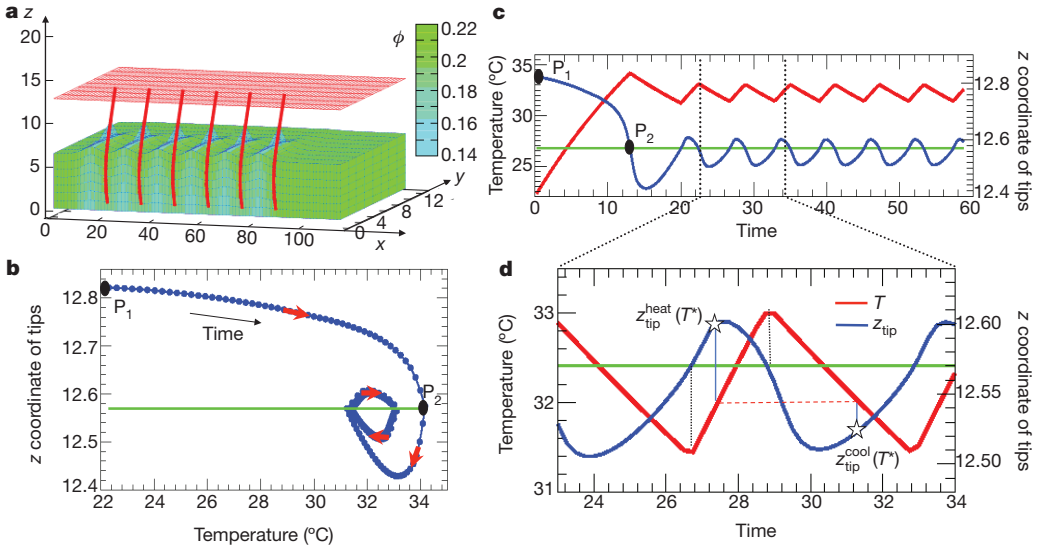

Figure 4 | Computer simulations of the self-sustained thermal regulation. **a**, Self-oscillations in SMARTS (microstructures, red; hydrogel, green; bilayer liquid interface, red plane). The colour bar indicates the volume fraction of polymer, ϕ, within the hydrogel. **b**, Phase trajectory $z_{tip}(T)$. The system follows the trajectory from left to right (see clockwise arrangement of arrows indicating the time direction). Point P_1 indicates the tip's initial height at 22 °C, and at point P_2 the tips first cross the interface. **c**, **d**, Time evolution of the z coordinate of the tips, $z_{tip}(t)$ (blue curve, right axis), and the temperature, $T(t)$ (red curve, left axis). The green line marks the position of the interface (red plane in **a**). In **d**, the stars mark the values $z_{tip}^{heat}(T^*)$ and $z_{tip}^{cool}(T^*)$, and indicate that at a fixed temperature the tips are higher during heating than cooling. In the undeformed state, the heights of the gel layer and posts are 18.6 and 25.6 μm, respectively, and the dimensionless unit of time corresponds to 4 s (Supplementary Information).

oscillation amplitude and period could be controlled by varying the position of the liquid–liquid interface, the geometry or mechanical properties of the microstructures, and the heating rate. The predicted trends were further confirmed by detailed experiments. Specifically, we note that the oscillation period gradually increases as the reactions progress; although the average period in reaction (i) was 4.20 min per cycle (Fig. 3c), it increased from the initial value of 3.58 min per cycle to 4.50 min per cycle as reactants were depleted (Supplementary Fig. 5c). Such an increase is in agreement with the predicted effect of varying the heating rate (Supplementary Fig. 10c), which depends on the reaction exothermicity and the reactant concentration. To study this effect further, we performed the hydrosilylation reaction with diluted reagents (80% v/v) and observed, as predicted, the increase in the initial oscillation period (to 3.85 min per cycle), as well as the decrease in the amplitude of both temperature oscillation (2.3 °C versus 2.8 °C) and tip position (~3 μm versus ~4 μm), as shown in Supplementary Fig. 6a. In contrast, when triethylsilane was replaced with diphenylsilane, which is more reactive, the higher heating rate resulting from a more vigorous reaction led to a shorter oscillation period (3.20 min per cycle) and a higher amplitude of both temperature oscillation (5.0 °C) and tip position (~7 μm) (Supplementary Fig. 6a). Similar results were obtained for SMARTS using other types of exothermic reactions (reactions (iii) and (iv)) (Supplementary Fig. 6b).

To study the correlation of the homeostatic performance and the position of the liquid interface, we raised the bilayer interface from ~12 to ~15 μm. With the higher interface, the microfins oscillated with a smaller amplitude of ~2 μm (versus ~4 μm) (Supplementary Fig. 7a). The temperature fluctuations were dampened as well, to an amplitude of 1.7 °C (versus 3.2 °C), around a slightly lower homeostatic point (32.0 °C compared with the original homeostatic point of ~32.7 °C), conceivably because the catalyst-coated microstructure tips remain in the reagent layer for shorter lengths of time when the interface is higher. All the latter effects of varying the interface position are also observed in our simulations (Supplementary Fig. 10a, b). To study the correlation of the homeostatic performance and microstructure size, 14.5-μm-tall microfins were used instead of the original 18.0-μm-tall ones. Reducing the fin height, while keeping the position of the liquid interface constant, resulted in the expected increase in the initial oscillation period (3.80 min per cycle) and the decrease in the actuation amplitude (to ~2 μm around a lower level of ~11 μm). At the same time, the temperature fluctuation amplitude increased to 5.0 °C (between 30.2 and 35.2 °C) (Supplementary Fig. 7b).

Our studies not only unravel the dynamic and collective responsiveness of SMARTS and the highly complex non-equilibrium behaviour that typifies its chemo-thermo-mechanical self-regulation, but also provide criteria for optimization and customization of its design. We demonstrated that the homeostatic temperature can be controlled by the LCST of the responsive gel; the frequency and amplitude of the autonomous temperature oscillation depend on the chemical reaction used and, for a given reaction, can be finely tuned by adjusting the height of the liquid interface, the rate of heat generation (through control of reagent concentration) or the microstructure dimension/geometry. We anticipate that the ability of SMARTS to maintain a stable temperature can be used in autonomous self-sustained thermostats with applications ranging from medical implants that help stabilize bodily functions to 'smart' buildings that regulate thermal flow for increased energy efficiency. In general, our rich SMARTS platform can involve a variety of other stimuli-responsive gels and catalytic reactions, enabling the creation of diverse homeostatic systems with various regulatory functions (controlling pH, light, glucose and pressure, for example). An oscillating mechanical movement originating from a non-oscillatory source, and leading to autonomous motility, has considerable potential for translation into areas such as robotics, biomedical engineering, microsystems technology and architecture, among many others. The system also can be used in the sensing and sorting of analytes in a microreactor device. The micrometre length scale, customizability and physical simplicity of SMARTS allow it to be integrated with other microscale devices, leading to far more complex self-powered, continuous or pulsed hierarchical chemomechanical systems capable of maintaining local state conditions.

METHODS SUMMARY

SMARTS fabrication. Microfins were made by polymerizing epoxy resin (UVO-114 with 10 wt% glycidyl methacrylate) within polydimethylsiloxane moulds that were replicated from silicon masters with corresponding geometry. Microfins were partly embedded in hydrogel by depositing an appropriate amount of hydrogel precursor solution on the microfin-bearing epoxy substrates and curing

under ultraviolet light. Microstructure tips were functionalized by stamping with a flat polydimethylsiloxane sheet inked with catalysts or fluorescence dye, and then thoroughly rinsing. To create a bilayer of aqueous liquids on top of the sample, the sample was integrated in a microfluidic device. Channels were laser-cut into acrylic, double-sided adhesive sheets and placed on top of the sample, and the channels were capped with polydimethylsiloxane allowing integration with polyethylene tubing, creating two inlets connected to two syringe pumps and an outlet. The height of the liquid–liquid interface was adjusted by changing the flow rates of the two ingoing solutions. To create a bilayer of organic–aqueous liquid, the two solutions of fixed volumes were sequentially placed on top of the microfins, forming a stable interface at a fixed height.

SMARTS characterization. Confocal microscopy was used to determine the position of the liquid interface and the tip positions of the actuating microfins. Optical imaging and video recording were done using an inverted microscope. Time-resolved temperature monitoring of SMARTS with incorporated exothermic reactions was carried out by precision fine wire thermocouples connected to a temperature controller and a computer.

Simulations. The gel lattice spring model[31–33] was extended to describe elastic filaments that are anchored within a thermo-responsive gel. The model takes into account heat produced by the exothermic reaction when the filament tips are above the reaction plane, as well as the heat dissipation throughout the system.

Received 18 November 2011; accepted 8 May 2012.

1. Bao, G. *et al.* Molecular biomechanics: the molecular basis of how forces regulate cellular function. *Cell. Mol. Bioeng.* **3,** 91–105 (2010).
2. Fratzl, P. & Barth, F. G. Biomaterial systems for mechanosensing and actuation. *Nature* **462,** 442–448 (2009).
3. Guyton, A. C. & Hall, J. E. *Human Physiology and Mechanisms of Disease* 6th edn 3–8 (Saunders, 1997).
4. Prosser, B. L., Ward, C. W. & Lederer, W. J. X-ROS signaling: rapid mechano-chemo transduction in heart. *Science* **333,** 1440–1445 (2011).
5. Sambongi, Y. *et al.* Mechanical rotation of the c subunit oligomer in ATP synthase (F0F1): direct observation. *Science* **286,** 1722–1724 (1999).
6. Spaet, T. H. Analytical review: hemostatic homeostasis. *Blood* **28,** 112–123 (1966).
7. Hess, H. Engineering applications of biomolecular motors. *Annu. Rev. Biomed. Eng.* **13,** 429–450 (2011).
8. Fritz, J. *et al.* Translating biomolecular recognition into nanomechanics. *Science* **288,** 316–318 (2000).
9. Lahann, J. & Langer, R. Smart materials with dynamically controllable surfaces. *MRS Bull.* **30,** 185–188 (2005).
10. Li, D. B. *et al.* Molecular, supramolecular, and macromolecular motors and artificial muscles. *MRS Bull.* **34,** 671–681 (2009).
11. Paxton, W. F., Sundararajan, S., Mallouk, T. E. & Sen, A. Chemical locomotion. *Angew. Chem. Int. Ed.* **45,** 5420–5429 (2006).
12. Sidorenko, A., Krupenkin, T., Taylor, A., Fratzl, P. & Aizenberg, J. Reversible switching of hydrogel-actuated nanostructures into complex micropatterns. *Science* **315,** 487–490 (2007).
13. Ariga, K., Mori, T. & Hill, J. P. Control of nano/molecular systems by application of macroscopic mechanical stimuli. *Chem. Sci.* **2,** 195–203 (2011).
14. Todres, Z. V. *Organic Mechanochemistry and its Practical Applications* (CRC/Taylor & Francis, 2006).
15. Harris, T. J., Seppala, C. T. & Desborough, L. D. A review of performance monitoring and assessment techniques for univariate and multivariate control systems. *J. Process Contr.* **9,** 1–17 (1999).
16. Stuart, M. A. C. *et al.* Emerging applications of stimuli-responsive polymer materials. *Nature Mater.* **9,** 101–113 (2010).
17. Yerushalmi, R., Scherz, A., van der Boom, M. E. & Kraatz, H. B. Stimuli responsive materials: new avenues toward smart organic devices. *J. Mater. Chem.* **15,** 4480–4487 (2005).
18. Das, M., Mardyani, S., Chan, W. C. W. & Kumacheva, E. Biofunctionalized pH-responsive microgels for cancer cell targeting: rational design. *Adv. Mater.* **18,** 80–83 (2006).
19. Murthy, N. *et al.* A macromolecular delivery vehicle for protein-based vaccines: acid-degradable protein-loaded microgels. *Proc. Natl Acad. Sci. USA* **100,** 4995–5000 (2003).
20. Nayak, S., Lee, H., Chmielewski, J. & Lyon, L. A. Folate-mediated cell targeting and cytotoxicity using thermoresponsive microgels. *J. Am. Chem. Soc.* **126,** 10258–10259 (2004).
21. Siegel, R. A. in *Chemomechanical Instabilities in Responsive Materials* (eds Borckmans, P., Kepper, P. D. & Khokhlov, A. R.) 139–173 (Springer, 2009).
22. Horváth, J., Szalai, I., Boissonade, J. & De Kepper, P. Oscillatory dynamics induced in a responsive gel by a non-oscillatory chemical reaction: experimental evidence. *Soft Matter* **7,** 8462–8472 (2011).
23. Kovacs, K., Leda, M., Vanag, V. K. & Epstein, I. R. Small-amplitude and mixed-mode pH oscillations in the bromate-sulfite-ferrocyanide-aluminum(III) system. *J. Phys. Chem. A* **113,** 146–156 (2009).
24. Maeda, S., Hara, Y., Sakai, T., Yoshida, R. & Hashimoto, S. Self-walking gel. *Adv. Mater.* **19,** 3480–3484 (2007).
25. Vanag, V. K. & Epstein, I. R. Resonance-induced oscillons in a reaction-diffusion system. *Phys. Rev. E* **73,** 016201 (2006).
26. Koga, S., Williams, D. S., Perriman, A. & Mann, S. Peptide-nucleotide microdroplets as a step towards a membrane-free protocell model. *Nature Chem.* **3,** 720–724 (2011).
27. Richter, A. *et al.* Review on hydrogel-based pH sensors and microsensors. *Sensors* **8,** 561–581 (2008).
28. Zarzar, L. D., Kim, P. & Aizenberg, J. Bio-inspired design of submerged hydrogel-actuated polymer microstructures operating in response to pH. *Adv. Mater.* **23,** 1442–1446 (2011).
29. Schild, H. G. Poly(*n*-isopropylacrylamide)-experiment, theory and application. *Prog. Polym. Sci.* **17,** 163–249 (1992).
30. Okano, T., Bae, Y. H., Jacobs, H. & Kim, S. W. Thermally on-off switching polymers for drug permeation and release. *J. Control. Release* **11,** 255–265 (1990).
31. Kuksenok, O., Yashin, V. V. & Balazs, A. C. Three-dimensional model for chemoresponsive polymer gels undergoing the Belousov-Zhabotinsky reaction. *Phys. Rev. E* **78,** 041406 (2008).
32. Yashin, V. V. & Balazs, A. C. Pattern formation and shape changes in self-oscillating polymer gels. *Science* **314,** 798–801 (2006).
33. Yashin, V. V., Kuksenok, O. & Balazs, A. C. Modeling autonomously oscillating chemo-responsive gels. *Prog. Polym. Sci.* **35,** 155–173 (2010).

Supplementary Information is linked to the online version of the paper at www.nature.com/nature.

Acknowledgements We thank P. Kim for assistance with the gel formulation, M. Khan for microstructure fabrication, R. S. Friedlander for assistance with confocal imaging, M. Kolle and A. Ehrlicher for technical assistance, and A. Grinthal for help with manuscript preparation. The work was supported by the US DOE under award DE-SC0005247 (experiment) and by the US NSF under award CMMI-1124839 (computational modelling).

Author Contributions M.A. and J.A. planned the project and supervised the research. X.H. and M.A. designed and conducted the experiments and data analysis. X.H., L.D.Z. and A.S. conducted the characterization. X.H. and L.D.Z. carried out microfluidic device design. A.S. carried out hydrogel deposition optimization. O.K. and A.C.B. developed the model and numerical code and carried out the computational simulations. All authors wrote the manuscript.

Author Information Reprints and permissions information is available at www.nature.com/reprints. The authors declare no competing financial interests. Readers are welcome to comment on the online version of this article at www.nature.com/nature. Correspondence and requests for materials should be addressed to J.A. (jaiz@seas.harvard.edu).